THE SEARCH FOR SWELLING CLAYS ALONG THE COLORADO FRONT RANGE:
THE ROLE OF AVIRIS RESOLUTION IN DETECTION

Sabine Chabrillat[1], Alexander F.H. Goetz[1,2]
1 Center for the Study of Earth from Space/CIRES, Campus Box 216,
2 Department of Geological Sciences,
University of Colorado, Boulder, CO 80309-0216 USA

1. INTRODUCTION

Swelling soils are a major geologic hazard, and expansive clays and clay-shales cause extensive damage world-wide every year. One of the worst swelling soils damage regions in the United States occurs along the 300 km long Front Range Urban Corridor in Colorado which is underlain by Cretaceous clay-shales, including the Pierre Shale. The sedimentary bedrock strata are generally flat-lying, except near the foothills of the Rocky Mountains where they have been uplifted into steeply-dipping strata. Expansive clays in the Pierre Shale and adjacent formations along the Front Range are responsible for the damage. The hazard is most severe in areas where these units dip steeply because of differential movement of adjacent beds (cm-m) which has been attributed to the abundance and composition of swelling clays (Gill *et al*., 1996). The three most important groups of clay minerals are smectite, illite and kaolinite. Smectite (including montmorillonite, the best-known member of the smectite group) has the greatest swelling potential and is responsible for most swelling soil damage in Colorado.

Current engineering and geologic practice for characterization of expansive clays involves time-consuming and expensive standard engineering tests for determination of swelling potential, and x-ray diffraction (XRD) analyses for mineralogical identification. Different types of clays can be identified spectroscopically thanks to their characteristic absorption bands around 2.2 μm. Reflectance spectrometry is then proposed as an alternate identification technique. At the laboratory /field scale, we use field spectrometers to relate spectroscopic features to mineralogical variations and degree of swelling potential. At the remote sensing scale, we investigate the potential of AVIRIS hyperspectral measurements to identify and map swelling soils and their swell potential.

2. LABORATORY /FIELD ANALYSES AND RESULTS

Good exposures of expansive clays along the Front Range Urban Corridor are limited in size and are sparse. Most of them are covered with grass, especially in the northern and Denver areas. South of Colorado Springs and around Pueblo and Canon City, exposures are more common and covered with desert-type vegetation. A total of 170 samples were collected at 30-50 cm depth from different locations shown in figure 1 on Hart's (1974) generalized geologic map. They were all taken from Upper Cretaceous Formations, Pierre, Niobrara, and Benton (younger to older). The great majority of samples obtained were clay-shales, consisting predominantly of mixed-layer illite/smectite with frequent thin bentonite beds (almost pure smectite, 10-30 cm thick), and are classified as having moderate to very high swell potential. Three types of analyses are performed on each sample, (a) geotechnical index tests including the Atterberg limits, grain size analysis, and one-dimensional swell test to determine the swelling potential; (b) XRD patterns on oriented samples to determine the mineralogical composition; and (c) reflectance spectra that are acquired in the VNIR-SWIR region. The laboratory analyses performed (XRD and swell tests) are described in more detail in Chabrillat et al., 1999.

Figure 2 shows reflectance spectra associated with field samples from the Denver Metropolitan area. Data were acquired in the laboratory with an ASD FieldSpec™ (www.asdi.com) and tungsten illumination. We focussed on the SWIR region since characteristic clay spectral features are found around 2.2 μm. The labels I to V refer to categories of swell potential following the classification proposed by MacKeen, 1992. Category I is for very high expansive potential, special cases, e.g. almost pure montmorillonite. Category II is for high expansive potential. Category III comprises moderate expansive potential, category IV low expansive potential. Category V soils are non-expansive. All spectra show some clay features, smectite for most of them (single well-defined absorption band at 2.2 μm, e.g. 96027), sometimes with illite (additional band at 2.35 μm, e.g. 96017), and sometimes with kaolinite (doublet band, e.g. 95022). They also all

show a deep water absorption band at 1.9 μm, which is indicative of the presence of montmorillonite in the samples. The spectra with a prominent smectite feature are associated with samples that are pure or almost pure smectite (99% to 100% smectite in clay fraction). These samples have very high swell potential. The spectra where illite can be detected with smectite are associated with the samples that have a high to moderate-low swell potential depending on the illite content. In general, more illite (less smectite) is associated with a lower swell potential. Kaolinite is detected in the spectra from samples which have a kaolinite content >10%, and where the swell potential is low to non-existent.

Working with our field samples from all along the Front Range Urban Corridor, from Canyon City and Pueblo to North Boulder, we observed that relationships between mineralogy, swell potential, and reflectance are multiple and complex, but follow some simple general rules: (a) from spectral reflectance we are able to discriminate among pure smectite and smectite/illite samples. The absorption band at 2.35 μm provides a measure of the illite content. The higher the amount of smectite (the less illite), the higher the swelling potential; (b) kaolinite is detected spectrally if above 10% in clay fraction in the sample. A significant amount of kaolinite (>10-15%) is indicative of low swelling potential. In the case of a significant content of kaolinite with pure smectite (case considered rare and unusual), the kaolinite doublet masks the smectite spectral feature at 2.2 μm, but the high amount of smectite (indicative of high swelling potential) can be spectrally detected in the limb of the 1.9 μm water absorption band.

Our goal now is to be able to apply these results at the remote sensing scale. The main difficulties which usually arise at this level are: (a) water absorption bands are masked by the atmospheric water vapor features; (b) natural surfaces are seldom perfect exposures of homogeneous expansive clays; and (c) the presence of vegetation can complicate the analysis.

3. AVIRIS IMAGERY

3.1 High and Low Altitude Data sets

AVIRIS scenes were acquired over the Front Range Urban Corridor in Colorado in late summer 1998, when the amount of green vegetation cover is at a near minimum. Six flight lines located in figure 1 were flown on September 10th. Most of them are cloud-free. Because of the mean ~1.7 km surface elevation in the area covered, the ER-2 flying at an altitude of 20 km provides a pixel size of ~17m x 17m and the swath width is ~10 km. The patial sampling is ~16m. Spectral data were acquired from 0.4 to 2.5 μm continuously with a spectral sampling of 10 nm.

As part of an experiment program, AVIRIS low altitude (AVIRIS-LA) images were acquired on October 21st 1998 over four sites along the northern part of the Urban Corridor. For this program the AVIRIS instrument was mounted on-board a NOAA Twin-Otter aircraft flying at an altitude of 3.8 km. GPS as well as pitch, roll and yaw data from a gyro system were recorded. The scenes swath width is ~1.2 km, and the pixel size is 1.9m x 1.9m. The spatial data are undersampled at an approximate rate of 1 every 3 pixel. Each AVIRIS-LA scene was corrected for pitch, roll and yaw and resampled by nearest neighbor (Boardman, 1999). The AVIRIS B-spectrometer was not working during this overflight. Spectral data were acquired with a 10 nm spectral sampling from 0.4 to 0.7 μm, and from 1.25 to 2.5 μm.

Figures 3a and 3b show associated AVIRIS high and low altitude images at 2 μm for the low altitude run 7 (Golden-Boulder) and run 9 (South Golden). The run 7 contains the kaolinite mine in the southern part, and Ralston reservoir in the northern part. This run is 9.5 km long, which gives an image size of ~500x5000 pixels for the low altitude data (~10 AVIRIS scenes), and ~55x550 pixels for the high altitude data. In the run 9 images we can see more man-made features, such as buildings, main (c470) and secondary roads. This second run is 6.6 km long and consists of ~7 low altitude scenes.

3.2 Calibration from radiance to Reflectance

Each AVIRIS scene was first radiometrically corrected by the Jet Propulsion Laboratory. The calibration of the data relative to ground reflectance was performed using the following procedure. For the high altitude data: (1) atmospheric correction using ATREM 3.0 (CSES, 1997) to model the solar irradiance; and (2) ground correction using field spectra acquired on the day and at the time of the overflight on an almost bare field calibration target in North Boulder. For the low altitude data, the loss of the B-spectrometer data prevented the use of ATREM for atmospheric modeling. We then

performed a straight ground correction using field spectra acquired on the day and time of the overflight on a gravel parking lot calibration target in South Golden.

Figure 4 shows the AVIRIS average reflectance spectra over a same site from the high and the low altitude data. This site, which is the Ralston reservoir dam, was not used in the calibration process. We can see that the spectra are coherent in shape and in level of reflectance.

3.3 Image Processing

As the goal of this study was to find and map expansive clay soils in the AVIRIS images, we applied the following procedure, using only the 2-2.45 μm spectral region:
1. A minimum Noise Fraction (MNF) transform was performed to determine and reduce the dimensionality of the data;
2. The Pixel Purity Index (PPI) method was used to find the most spectrally pure (extreme) pixels;
3. The extreme pixels were visualized in the data cloud from the ten first MNF bands. One of the clusters was identified as having pixels showing characterictic spectral clay features at 2.2 μm, such as kaolinite, smectite, and possibly illite;
4. Extreme clay pixels (endmembers) were extracted from the "clay" cluster;
5. A Mixture Tuned Matched Filtering (MTMF) method was eventually used to locate and map expansive clays outcrops. This last analysis provides an abundance map for each selected endmember associated with an "infeasibility" image to prevent detecting "false positives" in the original matched filtering algorithm (ENVI 3.1, www.rsinc.com).
The results from the high and low altitude data sets were compared in terms of the MNF bands, number of endmembers, extreme clays spectra, and abundance maps produced.

4. RESULTS

4.1 AVIRIS Mapping: Possibilities and Limitations

We focus here on the results from the high altitude data associated with the low altitude run 7. Figure 5 presents the three AVIRIS spectra associated with the endmembers selected in the clay cluster. From spectral identification, they are labeled as smectite (single band at 2.2 μm), illite/smectite (additional band at 2.35 μm), and kaolinite (doublet band). Figure 6 shows the abundance maps obtained with the MTMF algorithm for the three endmembers smectite (fig. 6a), illite/smectite (fig. 6b) and kaolinite (fig. 6c). The greyscale coding ranges from black (meaning that the spectrum of the associated pixel doesn't match with the endmember one, or abundance=0%) to white (meaning a perfect match between the spectra of the pixel and the endmember, or abundance=100%). In general, the location of all pixels coded from grey to light grey /white represents clay materials exposed in the image. The scattered nature of clay occurrences in the AVIRIS scenes is interpreted to be due to a predominance of non-clay materials at the ground surface (i.e., either vegetation cover or non-expansive, Quaternary-age alluvial deposits).

Figures 6a and 6b show that variable exposures of smectite and illite/smectite can be found mainly in the northern part of the scenes. This mapping coincides with our field observations, e.g. field work along the beaches of Ralston reservoir has shown that there are nicely exposed illite/smectite soils, with occasional rich smectite layers. Although the size of those outcrops is well below the spatial resolution of AVIRIS, the spectral resolution allows the identification of the clay signature occuring at the sub-pixel scale. The others locations where expansive clays were identified are associated in the field with natural outcropping areas, i.e. with a partial vegetation cover, such as grass or a few trees. Here also, we are able to extract the mineralogical spectral signature although there is mixing with other elements present in the pixels. Figure 6c shows that kaolinite is mapped only in the southern part of the image, around the kaolinite mine area. We did not detect any natural kaolinite outcrop. This mapping is confirmed by our field observations. If we apply our results from the laboratory analyses to interpret AVIRIS results in terms of swell potential, the northern areas are composed of expansive soils of variable swell potential. The highest swell potential outcrops are the ones mapped with the highest abundance in the endmember smectite, and the ones more abundant in the endmember illite/smectite are less swelling. Where there is some kaolinite mapped in the southern area, this area is low to non swelling.

In an attempt to quantify the possibilities and limits of AVIRIS detection of expansive clays, we studied a small Gronero shale outcrop in an area mapped in the low altitude run 9. This outcrop is well exposed, with almost no grass, but is small in size (~20m x 30m). The shales weather to dark grey soils, and the spectra from the field samples collected in similar-looking outcrops are very low in reflectance, <10% in the SWIR region. The same analysis described earlier was performed. Three extreme clay pixels associated with smectite, illite/smectite, and kaolinite were extracted from the data, and entered as endmembers in the MTMF. Abundance maps were produced. This outcrop was neither detected in the high altitude data (although other outcrops similar or smaller in size were detected), and nor in the low altitude data (where at this scale the outcrop consists of several pixels). Figure 7 shows AVIRIS-LA spectra associated with this outcrop. Two of them are from individual pixels, and the first one is the average of ~50 pixels associated with the whole outcrop. This figure demonstrates that the clay spectral feature *is* actually in the data, but because of the low reflectance level, we reach the detection limit in terms of signal-to-noise ratio (SNR). The spectral feature is at the same level as the noise for a single pixel. Averaging several pixels reduces the spatial resolution, but increases the SNR by the square root of the number of pixels, and therefore, the outcrop becomes detectable.

4.2 Comparison Between the High and Low Altitude Results: MNF Bands, Endmembers, and Abundance Maps.

Figures 8a and 8b show the ten first MNF bands associated with the high and low altitude data sets from run 7 and run 9 respectively. We have almost exactly the same MNF bands for run 7 and run 9 between the low and high altitude data. In the case of run 9 the low altitude data has more MNF eigenvalues than the high altitude data. There is only weeks between the two overflights, so the sun-angle difference is small, and even if there was any sun-angle factor affecting the MNF bands, we should observe it in both runs. This is not the case. The difference between the MNF eigenvalues in the high and low altitude data associated with run 9 is interpreted to be due to the increase in spatial resolution. This run contains many structures, such as roads, buildings, etc, which are resolved in the low altitude data and not in the high altitude ones. This difference is not observed in the data from run 7 which is composed mainly of natural occuring surfaces, such as rolling hills, grass, lakes and dams, covering large surfaces.

Figure 9 shows the three AVIRIS-LA spectra from run 7 associated with the endmembers selected in the clay cluster from the low altitude imagery. From spectral identification, they are labeled as smectite (single band at 2.2 μm), illite/smectite (additional band at 2.35 μm), and kaolinite (doublet band). Those spectra are to be compared with the ones in figure 5, extracted from the high altitude data over the same area. We can see that in both high and low altitude data we are able to extract the extreme, pure clay spectra, and that those signatures are coherent. Meanwhile, we observe also that the extreme spectra from the low altitude data are "purer", both in terms of level of reflectance and depth of absorption feature. Indeed, the low altitude spectra are, as expected, less mixed than the high altitude ones.

Figure 10 shows the abundance maps obtained from the low altitude imagery with the MTMF algorithm for the three endmembers smectite (fig. 10a), illite/smectite (fig. 10b) and kaolinite (fig. 10c). The greyscale coding is as described for figure 6. The abundance maps produced are roughly similar to the ones produced with the high altitude data, but more detailed in the low altitude data and with some differences in the abundances associated with the same areas on the ground. For example, if we compare figure 10a with figure 6a, the smectite endmember in the low altitude data is associated with a Ralston reservoir beach, although in the high altitude data the smectite endmember spectrum came from another location in the image. In the high altitude data we were able to detect the Ralston Reservoir beaches as smectite outcrops, but with a very low abundance (<30%), unlike the low altitude maps where the abundance is very high (60-100%). Inversely, the location from which the high altitude smectite endmember was extracted (abundance 80-100% in the high altitude smectite map) is identified in the low altitude data but with a much lower abundance (~40-60%). Those differences also can be seen very well in the kaolinite abundance maps (figure 10c and figure 6c), where in the high altitude data the whole kaolinite mine is mapped with a very high abundance (80-100%) although in the low altitude data only a few pixels are mapped with such a high abundance, and generally the whole kaolimite mine area is mapped with an variable abundance from 40 to 70%. The differences in the high and low altitude mapping are interpreted to be due to the differences in the spectrally pure (extreme) spectra used as image-endmembers in the MTMF algorithm. The abundance maps produced are relative to those spectra which are associated to more or less mixed surface on the ground. The purer the endmember spectrum, the more accurate the mapping.

5. SUMMARY

In summary, we are able to use spectral identification to discriminate among pure smectite and mixed smectite/illite samples. The higher the smectite content, the higher the swelling potential. The absorption band at 2.35 μm provides a measure of the illite content. Spectral detection of kaolinite is possible if it comprises above 10% in clay fraction, and a high content of kaolinite will be indicative of low swelling potential. Spectroscopic identifications of expansive clay field samples are well correlated with mineralogical x-ray diffraction analyses and geotechnical engineering tests. This work is still on-going as some discrepancies were observed, and we are working on the development of models to be able to predict the clay mineralogy and swell potential from the spectral signatures.

The analysis of the AVIRIS images (high altitude) showed that we were able, using a matched filtering algorithm, to identify the clay exposures among the other components in the image and despite the mixing at the sub-pixel scale (vegetation cover). A map of exposed clay material was produced. Among those exposures, spectral discrimination and identification of variable clay mineralogy (smectite, illite/smectite, kaolinite), related to variable swelling potential, is possible. The hyperspectral image analysis has then shown to be capable of detecting and mapping expansive clays, even at a 20m pixel size, in the presence of significant vegetation cover.

The comparison of the high altitude data with AVIRIS-LA images acquired at a spatial sampling of ~2m has proved to be very valuable, and has sometimes surprised us. Our analyses have shown that the increased spatial resolution (by a factor of 8 or so) provides less mixed endmembers, does not *necessarily* provide more endmembers among the images, and provides a more accurate mapping. To some extent, it raises the question of what is the more valuable, an increase in the spatial resolution or an increase in the SNR.

6. ACKNOWLEDGMENTS

7. REFERENCES

Boardman, J.W., 1999, "Precision Geocoding of AVIRIS low altitude data: Lessons learned in 1998", This Proceedings, AVIRIS Earth Science and Application Workshop, JPL, Pasadena, California, February 8-11 1999.

Center for the Study of Earth from Space (CSES), 1997, Atmosphere REMoval Program (ATREM), Version 3.0, University of Colorado, Boulder, 27pp.

Chabrillat S., A.F.H. Goetz, H.W. Olsen, L. Krosley and D.C. Noe, 1999, "Use of AVIRIS hyperspectral data to identify and map expansive clay soils in the Front Range Urban Corridor in Colorado", in Proceedings of the 13th Int. Conference on Applied Geologic Remote Sensing, Vancouver, Canada, March 1-3 1999, 8 pp.

Gill, J.D., M. W. West, D. C. Noe, H. W. Olsen and D. K. McCarty, 1996, "Geologic control of severe expansive clay damage to a subdivision in the Pierre Shale, Southwest Denver metropolitan area, Colorado", Clays and Clay minerals, vol. 44, no. 4, pp. 530-539.

Hart, S.S., 1974, "Potentially swelling soil and rock in the Front Range Urban Corridor, Colorado", Environmental Geology 7, 4 maps, scale 1:1,000,000, Colorado Geological Survey, Denver, CO.

McKeen, R.G., 1992, "A model for predicting expansive soil behavior", in Proceedings of the 7th Int. Conf. on Expansive Soils, Dallas, Texas, p. 1-6, August 3-5.
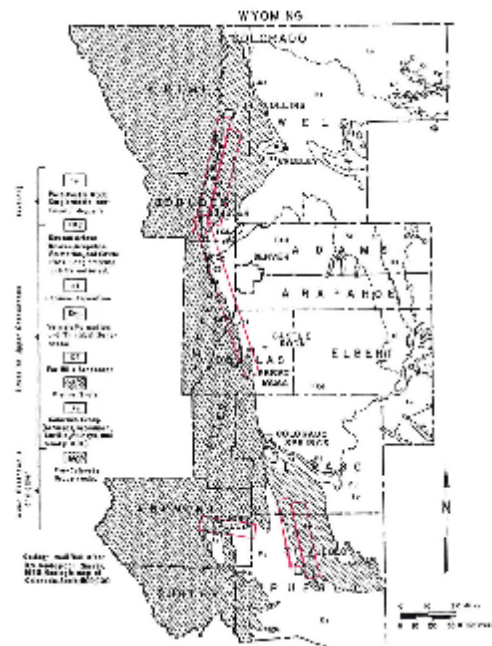
Figure 1. Generalized Geologic Map of the Colorado Front Range Urban Corridor (from Hart, 1974). Dashed areas locate Pierre Shale Formation. The $\otimes$ indicates field sampling location. The six frames locate the 1998 high altitude AVIRIS flight lines.
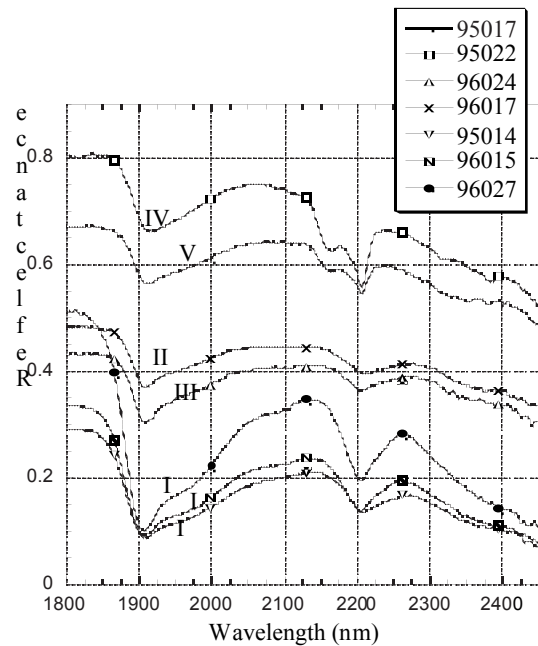

Figure 2. Laboratory reflectance spectra of field samples from Denver Metropolitan area. Labels I, II, III, IV and V are category of swell potential for each sample (from very high to low).
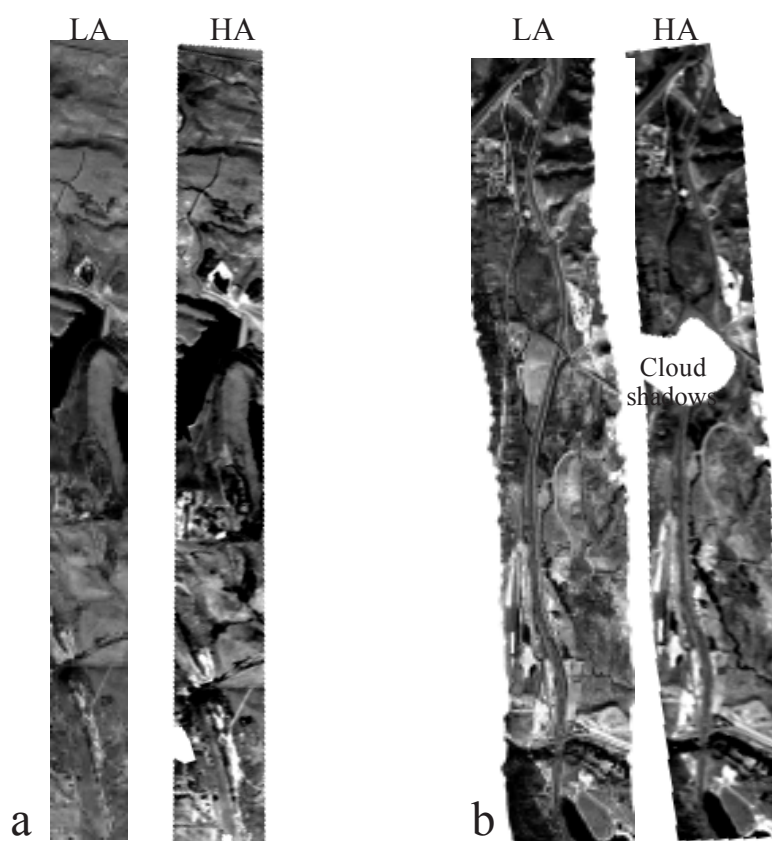
Figure 3. Associated High (HA) and Low (LA) altitude AVIRIS images at 2 μm.
a- Low altitude run 7, Golden-Boulder; b- Low altitude run 9, South Golden (c470).
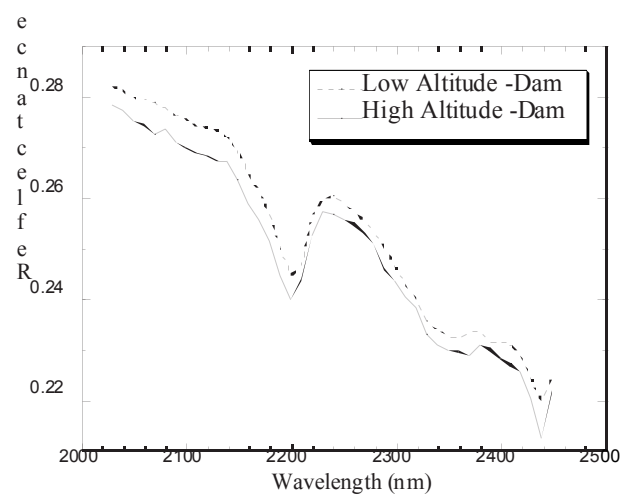
Figure 4. Calibration to reflectance. Comparison of high and low altitude.
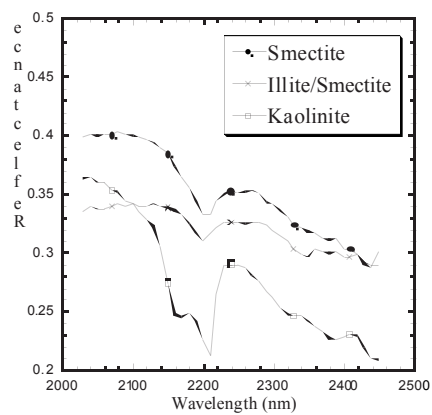AVIRIS average spectra over Ralston Reservoir Dam.

Figure 5. AVIRIS spectra of the three clay endmembers (SWIR).
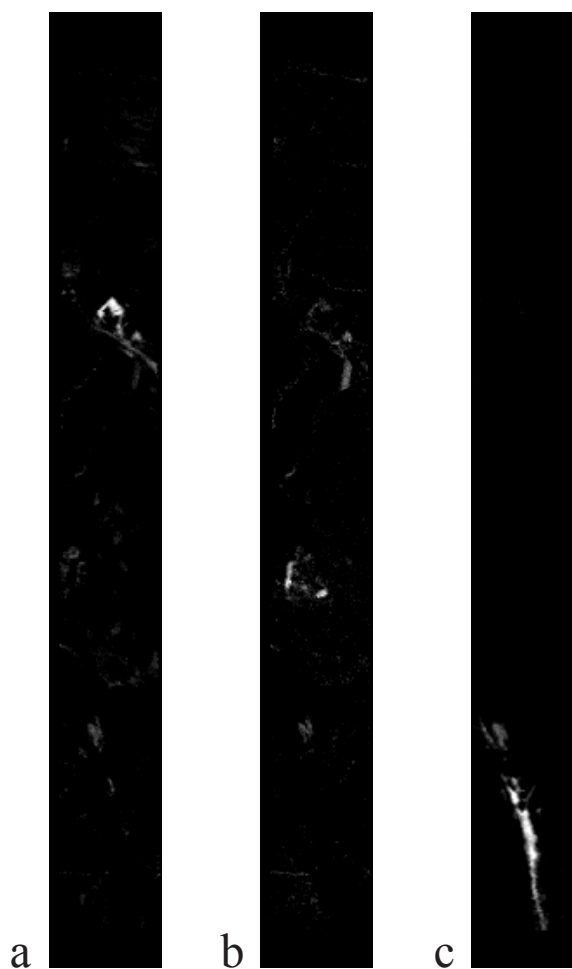High altitude data.

a   b   c

Figure 6. Abundance maps obtained with the mixture tuned matched filtering algorithm
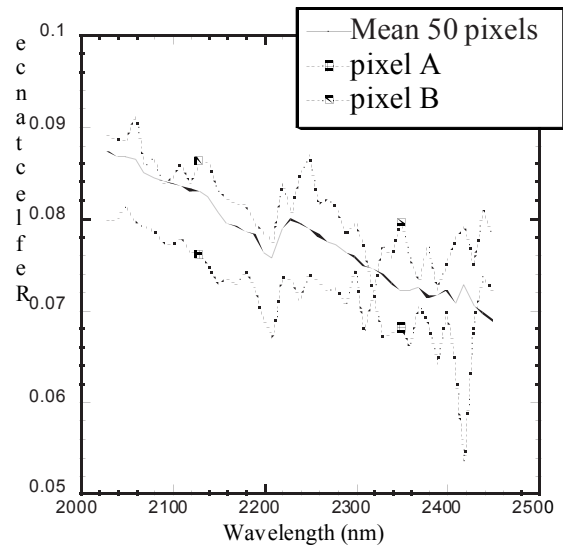For the three endmembers (figure 5). a- smectite, b- illite/smectite, c- kaolinite.

Figure 7. AVIRIS-LA spectra over the Gronero Shale outcrop (detection test site).
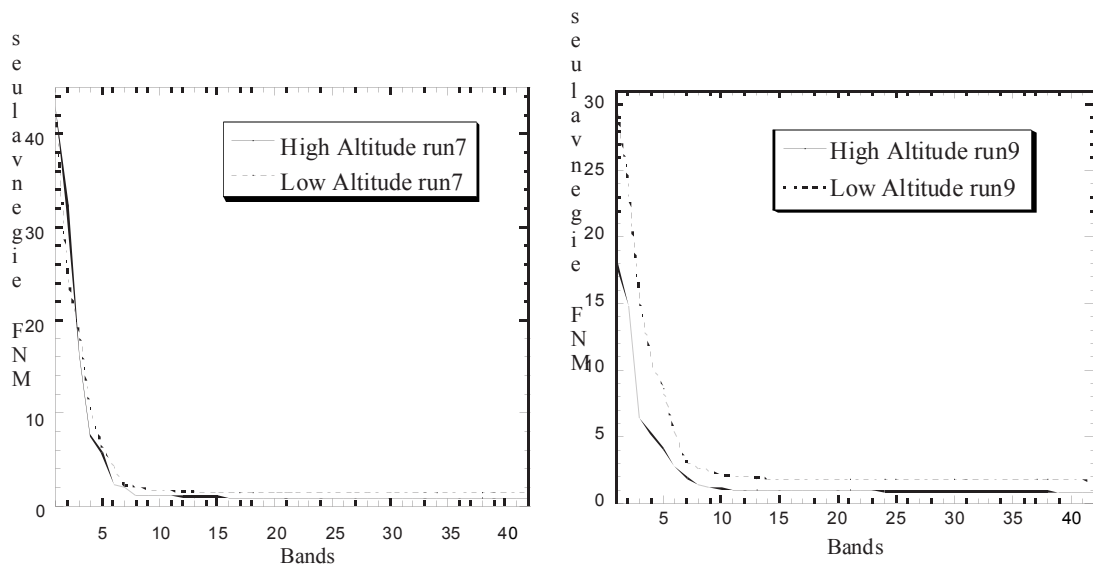

Figure 8. Comparison of the high and low altitude MNF bands.
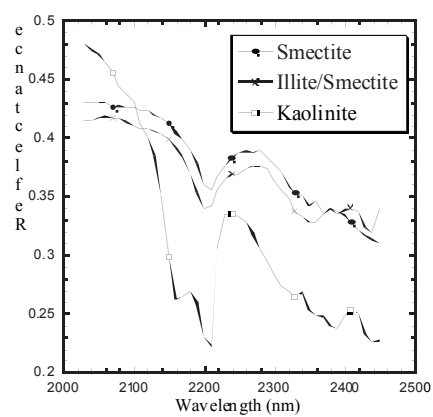a- low altitude run 7, b- low altitude run 9.

Figure 9. AVIRIS-LA spectra of the three clay endmembers (SWIR).

a   b   c

Figure 10. Abundance maps obtained with the mixture tuned matched filtering algorithm
For the three endmembers (figure 9). a- smectite, b- illite/smectite, c- kaolinite.